



**HAL**  
open science

## Thermal structural ratcheting simulation-Evaluation of industrial-used constitutive models

Jean Macedo, Jean-Michel Bergheau, Stéphane Chapuliot, Eric Feulvarch, Olivier Ancelet, Antoine Martin

► **To cite this version:**

Jean Macedo, Jean-Michel Bergheau, Stéphane Chapuliot, Eric Feulvarch, Olivier Ancelet, et al.. Thermal structural ratcheting simulation-Evaluation of industrial-used constitutive models. Thin-Walled Structures, 2023, 182- Part B, pp.110301. 10.1016/j.tws.2022.110301 . hal-04801809

**HAL Id: hal-04801809**

**<https://hal.science/hal-04801809v1>**

Submitted on 25 Nov 2024

**HAL** is a multi-disciplinary open access archive for the deposit and dissemination of scientific research documents, whether they are published or not. The documents may come from teaching and research institutions in France or abroad, or from public or private research centers.

L'archive ouverte pluridisciplinaire **HAL**, est destinée au dépôt et à la diffusion de documents scientifiques de niveau recherche, publiés ou non, émanant des établissements d'enseignement et de recherche français ou étrangers, des laboratoires publics ou privés.

# Thermal structural ratcheting simulation - Evaluation of industrial-used constitutive models

Jean Macedo<sup>a,b,\*</sup>, Jean-Michel Bergheau<sup>b</sup>, Stéphane Chapuliot<sup>c</sup>, Eric Feulvarch<sup>b</sup>, Olivier Ancelet<sup>a</sup> and Antoine Martin<sup>a</sup>

<sup>a</sup>Framatome, France

<sup>b</sup>University of Lyon, EC-Lyon, LTDS, UMR5513 CNRS, Saint-Etienne, France

<sup>c</sup>EDF Group, France

---

## ARTICLE INFO

### Keywords:

Ratcheting  
Elastoplastic material  
Constitutive models  
Thermomechanical loading  
Structural ratcheting experiment

---

## ABSTRACT

This article presents an evaluation of the performance of conventional constitutive models in modelling the structural ratcheting of an austenitic stainless steel structure subjected to a thermomechanical loading. This work highlights the influence of monotonic and cyclic behaviour in ratcheting responses. Propositions on how to determine constitutive models and which ones are able to reproduce ratcheting responses are also presented. Models employing only kinematic hardening are found to be inadequate in predicting structural ratcheting. Results predicted by a simplified version of Chaboche model proposed here are found in good agreement as compared to experimental measurements.

---

## 1. Introduction

When a structure is subjected to a cyclic loading with non-zero mean stress, the accumulation of plastic strain may not cease after a significant number of cycles and it will lead the structure to failure. This phenomenon is known as ratcheting (Fig. 1). For nuclear power plant components, ratcheting occurs mainly as a result of the combination of an internal pressure and a cyclic thermal loading. In that case, one is talking about the thermal ratcheting phenomenon. According to nuclear design codes (RCC-M, RCC-MRx, ASME, KTA, ...), the structures of a nuclear power plant which are subjected to that kind of loadings require the performance of a ratcheting check. This check can be investigated by means of simplified methods or a complete inelastic analysis [1, 2]. On the one hand, the latter is less conservative, but on the other hand, it is more computationally expensive than the former.

Depending on the loadings conditions and structure's geometry, this complex cyclic phenomenon can be classified as a material or a structural ratcheting [3]. The former and the latter may also be referenced as local and global, respectively, in the literature [4]. Material ratcheting is characterized by a homogeneous stress state while the structural ratcheting is related to the structural effects (i.e., an inhomogeneous stress state). In the last decades, ratcheting experiments, for austenitic stainless steel materials, have been carried out to better understand these two ratcheting mechanisms.

Material ratcheting is observed in laboratory experiments such as an asymmetrical. Hassan et al. [5] carried out uniaxial stress-controlled experiments in order to investigate ratcheting in 304 stainless steel specimens. They observed that cyclic hardening reduce the ratcheting rate over cycle.


Portier et al. [6] conducted a series of uniaxial and biaxial ratcheting experiments in 316 austenitic stainless steel specimens. These experiments have evidenced the effects of uniaxial and biaxial ratcheting. Facheris et al. [7] performed uniaxial and biaxial experiments to study the effect of ratcheting on fatigue life. The ratcheting behaviour of a straight pipe under both an uniaxial loading and an internal pressure was investigated by [8, 9, 10]. The axial and hoop ratcheting of straight pipe under cyclic bending [11] and under both cyclic bending and an internal pressure [12, 13] have also been analysed. More recently, uniaxial ratcheting tests have been carried out to observe the influence of the dynamic strain aging (DSA) in ratcheting phenomenon [14, 15, 16]. Also, elbow pipe has been tested in order to study the influence of ratcheting on the ovalization of cross-section [17].

Despite these ratcheting experiments have contributed to understand the material ratcheting, they were not representative of the ratcheting phenomenon observed on nuclear structures (i.e., they did not highlight neither the thermal ratcheting nor the structural ratcheting). To investigate the thermal ratcheting effects that are mainly induced by thermomechanical loadings, Uga [18] and Taleb [19] developed thermal ratcheting facilities. Bars or concentric tubes were submitted to homogenous thermomechanical loading. Their experiments had confirmed that the combination of a constant mechanical loading and a cyclic thermal loading creates an incremental plastic strain cycle after cycle. Nevertheless, structural effects were not emphasized on these tests.

To analyse both the thermal ratcheting and structural effects, it is necessary to conduct a structural ratcheting test. Even though its complexity, a few structural ratcheting experiments were developed. Couterot [20] carried out a complex experiment on a representative mock-up to analyse structural ratcheting. Because of the low plastic strain accumulation, the ratcheting was not evidenced in his test. Another structural ratcheting test was proposed by the

---

\* Corresponding author.

 jean-caio.macedo-alves-de-lima1@framatome.com (J. Macedo)

ORCID(s):

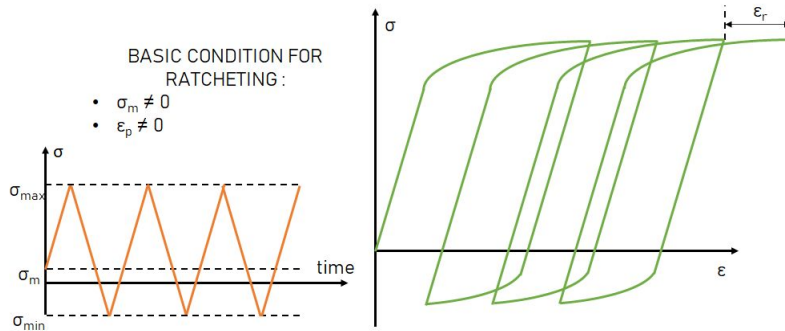


Figure 1: Illustration of ratcheting phenomenon.

French Alternative Energies and Atomic Energy Commission (CEA): the COTHAA test. Submitting a cylindrical structure to a cyclic thermal gradient under a constant internal pressure, an accumulation of hoop plastic strain is observed through the cycles. Due to the thermomechanical loading and the specimen's geometry, the latter has been used in nuclear industry to understand the structural ratcheting and to evaluate the conservatism of simplified methods to assess it [21, 22].

Concerning the cyclic inelastic analyses, efforts have been made in order to improve constitutive models in predicting ratcheting. In general, kinematic hardening rule is used to simulate ratcheting. Prager [23] was the first which came up with a linear hardening rule to consider the baushinger effect. The plastic modulus calculation in this model is coupled with its kinematic hardening rule through the consistency condition. To better simulate cyclic plasticity, Armstrong-Frederick [24] proposed a non-linear hardening rule. Despite that improvement, these models are well known for either underpredicting or overpredicting ratcheting, respectively. Thus, Armstrong-Frederick model has been modified [25, 26], in particular the non-linear part, in order to avoid the overprediction of both material and structural ratcheting. On the other hand, Mroz [27, 28] and Guard [29] proposed a multi-surface model that the plastic modulus calculation is indirectly coupled with its kinematic hardening rule. The latter is not analysed in this work.

The aim of this paper is to propose a robust constitutive model capable of simulating ratcheting with accuracy and a strategy to determine their parameters from material data. The paper is composed of 6 sections. The section 2 presents the structural ratcheting experiment known also as COTHAA test. The section 3 is addressed to the constitutive models which are often used to simulate ratcheting and the methodology used to identify their parameters. The section 4 describes the FE model. The section 5 is dedicated to the FEA. The evaluation of constitutive models are presented and discussed. Finally, section 6 concludes with suggestions for future work.

## 2. COTHAA device

An experimental ratcheting device, called COTHAA, was developed to analyse the structural ratcheting phenomenon [21]. A representative cylindrical structure is heated by Joule effect and subjected to a constant internal pressure in order to get closer from a representative case of a nuclear power plant. The aim of this experimental campaign was to investigate the commonly-used ratcheting design rules. As the latter are based on simplified assumptions, it was observed that they are too conservatives [22]. Here, COTHAA device is presented as well as the specimen's material and geometry.

### 2.1. Material and specification

The specimens used for the experimental investigations were made of a 316L austenitic stainless steel. This material is a representative of nuclear grades. Its chemical composition is listed in Table 1.

As thermomechanical calculations are performed, both thermal and mechanical properties are required. Furthermore, the heating is created by Joule effect thus, an electrical property is essential: the electrical conductivity. Also, because of the 316L material is considered temperature-dependent, their properties vary according to the temperature.

Electrical and thermal properties are reported in Table 2, in which  $T$  denotes the temperature,  $\sigma$  the electrical conductivity,  $\rho$  the density,  $c_p$  the specific heat and  $\lambda$  the thermal conductivity. Mechanical properties are listed in Table 3, where  $E$  is the Young's modulus,  $R_{p0.2\%}$  is the yield stress defined at 0.2% plastic strain and  $\alpha$  is the thermal expansion coefficient. Due to the lack of experimental data, thermal and mechanical properties are taken from the RCC-MRx code [30] and the electrical conductivity from [31].

Two kinds of geometry were used and those geometries are mainly distinguished by their thickness transition zone: with an abrupt change of cross-section and with similar transitions of the nuclear components. Only the experimental tests with abrupt changes of thickness are here treated. That geometry is presented in Fig. 2.

**Table 1**

316L chemical composition (wt%) .

C	Mn	S	P	Si	Cr	Ni	Mo	Co
0.018	1.620	0.002	0.024	0.350	16.700	11.080	2.130	0.200

**Table 2**

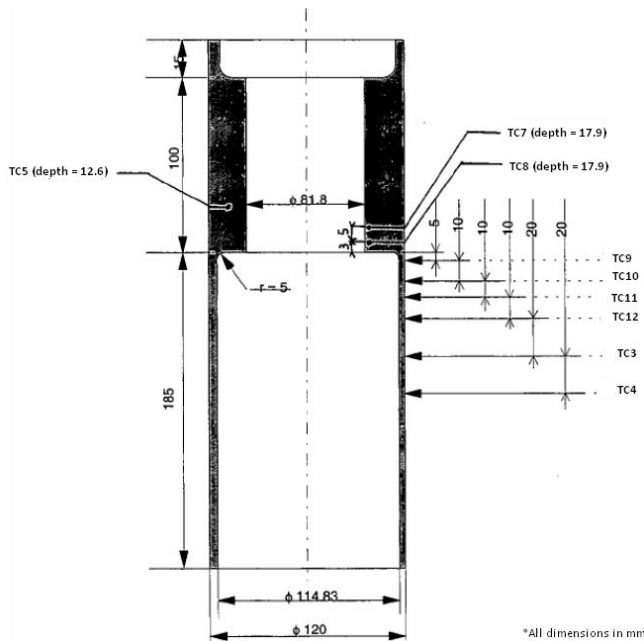
Electrical and thermal properties [30, 31].

T (°C)	$\sigma$ (S/m)	$\rho$ (kg/m <sup>3</sup> )	$\lambda$ (W/m.K)	$c_p$ (J/kg.K)
20	1303968	7930	14.28	472
100	1199863	7899	15.48	501
200	1112176	7858	16.98	522
300	1043599	7815	18.49	538
400	989992	7770	19.99	556
500	952375	7724	21.49	590

**Table 3**

Thermomechanical properties [30].

T (°C)	E (GPa)	$R_{p0.2\%}$ (MPa)	$\alpha$ (10 <sup>-6</sup> /°C)
20	200	235	15.3
100	193	196	15.9
200	185	159	16.6
300	176	135	17.2
400	168	120	17.8
500	159	110	18.3


**Figure 2:** COTHAA geometry and thermocouple positions extracted from [21].

## 2.2. Experimental setup

The specimens were machined from a 316L nuclear pipe and heat treated in order to ensure the initial properties of the material. After that, the tests were performed.

The COTHAA experiment was divided into three phases. First all, the COTHAA structure was pressurized using a gas system. Then, a high-intensity current was applied to the structure, causing the structure's heating by means of the Joule effect. The heating goes on for twenty seconds, when a predefined temperature is reached on the geometry's thinnest part. For the numerical model, an electric potential difference is applied between the bottom and the top of the specimen to achieve this prescribed temperature (see section 4.1). Finally, the heating was stopped and cooling by natural convection was started until the temperature of 50°C was reached in around 1500 seconds. After that, a new cycle could be initiated.

Analyzing the thermomechanical effects, one can observe that the thinnest part of the structure heats faster than the thickest one during the heating phase. Because of that, a thermal gradient is created around the zone of cross-section change. Hence, this phenomenon over the cycles creates an asymmetrical reversed bending stress that induces an increase of the structure's diameter at the end of each cycle. In other words, it produces an accumulation of the hoop plastic strain or a hoop ratcheting. The four COTHAA experiments investigated on this work are summarized in the Table 4, where set T denotes the set temperature and  $p_i$  the internal pressure. The COTHAA experiments will then be referenced according to their test reference (Table 4 first column).

The temperature was readout from nine thermocouples (Fig. 2). Those were placed in/on the structure along its axial direction to quantify and characterized the temperature field. The thermocouple's name are also referenced as TCx, in which x represents its number according to the Fig. 2. The time-measured temperature curves of the test 8 experiment is given in Fig. 3. Moreover, the set temperature, presented in Table 4, was readout from the TC12.

The hoop ratcheting was measured using a profilometer equipment. The measurements were made on the cylinder's external generatrix at the end of the cycle 1, 2, 5, 10, 20, 30 until the hoop ratcheting stabilization (Fig 4). Note that all these measurements were made without applying the internal pressure and at room temperature. Fig. 5 gives the evolution of the maximal hoop strain, on the cylinder's external generatrix, over the cycles.

**Table 4**

COTHAA experiments [22].

Test reference	set T (°C)	$p_i$ (MPa)
7a	415	4.8
8	450	4.5
11a	360	4.5
12a	270	4.5

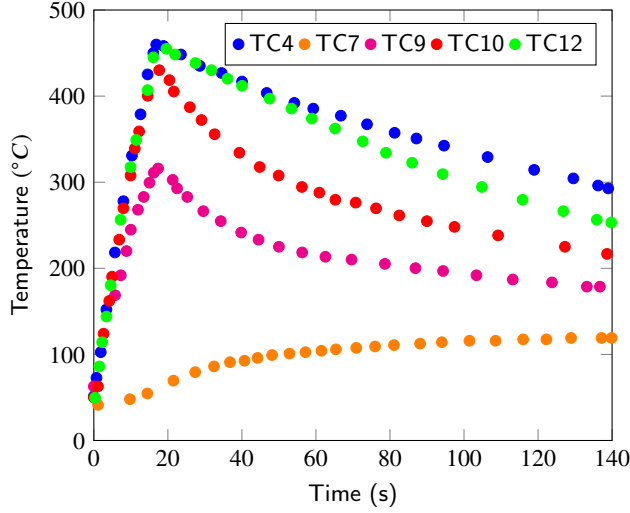


**Figure 3:** Time-temperature evolution throughout the heating and the beginning of the cooling by natural convection of the test 8.

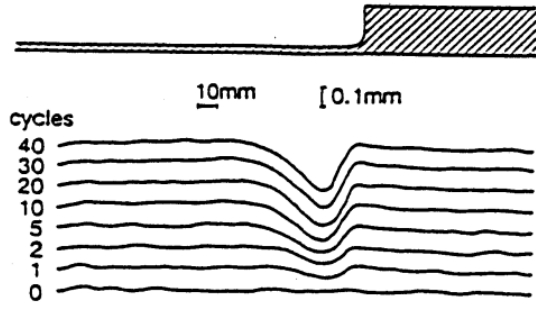


**Figure 4:** Profilometer measurements of test 8 extracted from [22].

### 3. Constitutive models and their determination

#### 3.1. Cyclic plasticity

The cyclic plasticity constitutive models used for ratcheting analyses with the assumption of rate-independent plasticity consist of the following conditions:

$$\dot{\epsilon} = \dot{\epsilon}^e + \dot{\epsilon}^p \quad (1)$$

$$\sigma = \mathbf{C} : \epsilon^e \quad (2)$$

$$\dot{\epsilon}^p = \dot{\lambda} \frac{\partial f}{\partial \sigma} = \sqrt{\frac{3}{2}} \dot{\lambda} \mathbf{n} \quad (3)$$

$$f(\sigma - \mathbb{X}) = \sqrt{\frac{3}{2} (\mathbb{S} - \mathbb{X}) : (\mathbb{S} - \mathbb{X})} - (\sigma_y + R) \quad (4)$$

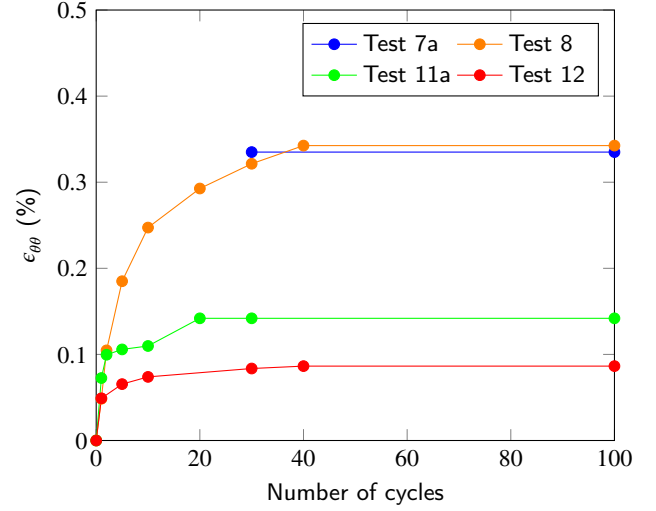


**Figure 5:** Maximal hoop ratcheting over the cycles.

where Eq. (1) represents the strain-rate decomposition  $\dot{\epsilon}$  into a elastic part  $\dot{\epsilon}^e$  and an plastic part  $\dot{\epsilon}^p$ . The elastic strain obeys the Hooke's law (2) while the plastic one is based on the flow law (3). Also,  $\mathbf{C}$ ,  $\dot{\lambda}$  and  $\mathbf{n}$  indicate the fourth-order elasticity tensor, the plastic multiplier and the outward unit normal vector to the yield surface, respectively. Finally, Eq. (4) corresponds to the von Mises yield criterion, where  $\mathbb{S}$  is the deviatoric stress tensor,  $\mathbb{X}$  is the back-stress tensor (or kinematic hardening tensor), which describes the yield surface translation,  $\sigma_y$  is the initial yield stress and  $R$  the isotropic hardening, which describes the increase/decrease of the yield surface's size.

Concerning the kinematic hardening, it is considered to be the primary reason for ratcheting. As a result, a lot of kinematic hardening rule have been suggested to model ratcheting. Prager [23], in the authors' knowledge, was the first author to proposed that kind of a model: the linear kinematic hardening rule in the form:

$$\mathbb{X} = \frac{2}{3} C \epsilon^p \quad (5)$$

where  $C$  is a material dependent parameter.

Due to its linear form, this model is well known to be unable to reproduce neither the experimental hysteresis curves nor the material ratcheting. Hassan [32] demonstrated that this model leads to a plastic shakedown after the first cycle, for an uniaxial ratcheting test, or after a few cycles, for a biaxial ratcheting test.

To improve cyclic plasticity modelling, Armstrong-Frederick [24] introduced a non-linear part in the Prager model (5), called dynamic recovery:

$$\dot{\mathbb{X}} = \frac{2}{3} C \dot{\epsilon}^p - \gamma \mathbb{X} \dot{p} \quad (6)$$

where the new parameter  $\gamma$  is a material dependent coefficient and  $\dot{p}$  is the equivalent cumulative plastic strain

rate that is defined in Eq. (7). From the consistency condition  $\dot{f} = 0$ , one deduces that  $\dot{p}$  is here identical to the plastic multiplier  $\dot{\lambda}$ .

$$\dot{p} = \sqrt{\frac{2}{3} \dot{\epsilon}^P : \dot{\epsilon}^P} \quad (7)$$

The Armstrong-Frederick model, also termed as non-linear kinematic hardening rule or AF, predicts the strain-controlled curves better than the former. Due to the recall term, the shape of the kinematic hardening rule changes between tension and compression. As a result, when imposing asymmetric uniaxial stress cycles, the hysteresis loops never close and a constant ratcheting-rate is produced. The constant ratcheting-rate, for uniaxial stress-controlled tests, is given in Eq. (8), where  $X_{min}$  represents the back-stress in compression and  $X_{max}$  the back-stress in tensile. All these effects were demonstrated in [32].

$$\dot{\epsilon}_{ratcheting}^P = \frac{1}{\gamma} \ln \left( \frac{X_{min}^2 - (C/\gamma)^2}{X_{max}^2 - (C/\gamma)^2} \right) \quad (8)$$

To better simulate ratcheting, Chaboche [33, 34] proposed the combination of two or more hardening kinematic rules. Its generalize formulation is given as follows:

$$\dot{\mathbb{X}} = \sum_{i=1}^n \left( \frac{2}{3} C_i \dot{\epsilon}^P - \gamma_i \mathbb{X}_i \dot{p} \right) \quad (9)$$

The incorporation of several kinematic rules allows the Chaboche model to simulate uniaxial ratcheting responses better than the previous models. However, for multiaxial loading, ratcheting simulation is still overpredicted. Hassen [32] observed that the Chaboche model with  $n = 3$  or  $n = 4$ , predicts reasonably the uniaxial ratcheting, but still overestimates the biaxial one.

For a long time, the isotropic hardening, attributed to be the secondary reason for ratcheting, was not considered on ratcheting evaluations. Recently, authors have mentioned that its incorporation in constitutive models seems to be an improvement in ratcheting simulations [32, 12]. Hence, the isotropic hardening effect in ratcheting simulation is tested in this paper.

The commonly-used isotropic hardening rule, proposed by Chaboche [25, 35], is here presented. As stated before, the isotropic hardening corresponds to an increase (hardening) or a decrease (softening) of the material's yield surface size. Its evolution is defined as follows:

$$\dot{R} = b(Q - R)\dot{p} \quad (10)$$

where  $b$  and  $Q$  are material dependent coefficients.  $b$  controls the stabilization-rate and is determined from a regression analysis of the uniaxial hysteresis loops.  $Q$  is the asymptotic value of  $R$ . For exemple, when the material

stabilization is achieved, for a symmetrical uniaxial loading, the yield stress is equal to  $\sigma_y + Q$ . In addition, the material hardens if  $Q > 0$  or softens if  $Q < 0$ .

Experimental observations demonstrated that the asymptotic value  $Q$  depends on the plastic strain range. However, since  $Q$  saturates for the first plastic strain applied, Eq. (10) cannot reproduce the behaviour observed in Fig. 6.

To mitigate that, Chaboche [33] proposes the introduction of a plastic strain range memorisation, which relates  $Q$  with the plastic strain range applied. This formulation is depicted as follows:

$$F = \sqrt{\frac{2}{3} (\epsilon^P - \zeta) : (\epsilon^P - \zeta)} - q \quad (11)$$

$$\dot{q} = \eta H(F) \langle \mathbf{n} : \mathbf{n}^* \rangle \dot{p} \quad (12)$$

$$\dot{\zeta} = \sqrt{\frac{3}{2}} (1 - \eta) H(F) \langle \mathbf{n} : \mathbf{n}^* \rangle \mathbf{n}^* \dot{p} \quad (13)$$

$$\mathbf{n}^* = \sqrt{\frac{3}{2}} \frac{\epsilon^P - \zeta}{\sqrt{\frac{3}{2} (\epsilon^P - \zeta) : (\epsilon^P - \zeta)}} \quad (14)$$

Analogous to Eq. (4), Eq. (11) describes the memory surface and the parameters  $q$  and  $\zeta$  represent the size and the center of this surface. The material dependent coefficient  $\eta$  is used to describe the kinetic of the strain memorisation. For instance, with  $\eta = 0.5$ , one obtains an instantaneous memory and the stabilization is reached once the first cycle is performed.

Similar to  $\mathbf{n}$  (Eq. (3)),  $\mathbf{n}^*$  is the the outward unit normal vector to the memory surface. Furthermore,  $\langle . \rangle$  indicates the Macaulay bracket and  $H$  the Heavside function.

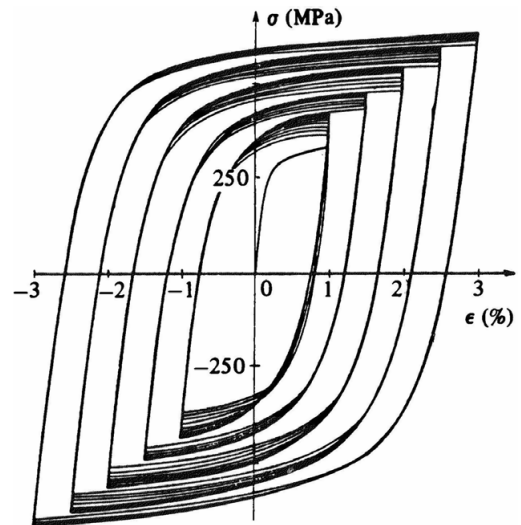


Figure 6: Uniaxial strain-controlled test of a 316L material at room temperature, extracted from [33].

The relation between  $Q$  and  $q$  is defined as:

$$Q = 2\beta(Q_M - Q)\dot{q} \quad (15)$$

where  $Q_M$  corresponds to the asymptotic value of  $Q$  for a maximum strain range applied during an uniaxial test.

### 3.2. Constitutive models evaluated

Constitutive models, that have had their performance in predicting ratcheting under mechanical loadings explored in the literature, do not account for loadings observed on a nuclear component. Therefore, one of the contributions of this work is to extend the robustness evaluation of constitutive models in predicting ratcheting under a thermomechanical loading. For this purpose, three models are selected to be confronted with COTHAA test.

**Double Armstrong-Frederick model**, also referenced as 2AF model in this study, is a superposition of two Armstrong-Frederick hardening rules,  $n = 2$  in Eq. (9).

**Armstrong-Frederick-Prager model**, also mentioned here as AFP model, is also a superposition of two kinematic hardening rules with a value of  $\gamma_2$  sets to 0. The combination of a linear and non-linear kinematic hardening reduces the ratcheting-rate.

**Simplified Chaboche model**, is called SC model in this work, is proposed as a combination of the AFP model and the isotropic hardening rule with a plastic strain range memorisation (Eqs. (10)-(14)).

### 3.3. Model parameters determination

The model parameters are calibrated from data sets of monotonic tensile tests or uniaxial tests. From uniaxial strain-controlled tests, a cyclic curve may be defined as the relation between the applied strain range and the stabilized stress. Fig. 7 illustrates the difference between monotonic, cyclic and stabilized curves.

The experimental data is fitted to the model parameters to a mathematical model according to the least-squares method. The mathematical models of the three models are treated by Chaboche [35] and can be deduced from (3)-(15).

For the 2AF model and AFP model, two set of parameters were determined: one from cyclic curves data and another from monotonic curves data. Models identified from cyclic curves are referenced here with a index 1. On the other hand, those with a index 2 were identified from monotonic curves. These determinations are made using Eqs. (16) and (17).

For the SC model only one set of parameters was determined. The SC model determination is divided into two phases. First, the kinematic hardening parameters are determined using the same method as AFP-2 model. Secondly, isotropic hardening parameters are calibrated from cyclic curves, this time using (18). Finally, the kinetic parameters  $b$ ,  $\eta$  and  $\beta$  are calibrated from the test 8.

Table 5 summarizes the models evaluated as well as the material curves used to determine them. The first column represents the model and the first row the material data.

Comparisons between experimental curves and the models are presented in figures 8-9. Except for the SC model, for which the consideration of cyclic hardening led to a monotonic curve that overestimates high plastic strains, all the models are consistent with the experimental curves. Note that all these models are determined according to the temperatures listed on the first column of the Table 3, however, for clarity reasons only the results at room temperature and at 300°C are presented in this section.

$$\sigma = \sigma_y + \frac{C_1}{\gamma_1} (1 - \exp(-\gamma_1 \varepsilon^p)) + \frac{C_2}{\gamma_2} (1 - \exp(-\gamma_2 \varepsilon^p)) \quad (16)$$

$$\sigma = \sigma_y + \frac{C_1}{\gamma_1} (1 - \exp(-\gamma_1 \varepsilon^p)) + C_2 \varepsilon^p \quad (17)$$

$$\frac{\Delta\sigma}{2} = \sigma_y + Q_0 + \frac{C_1}{\gamma_1} \tanh\left(\gamma_1 \frac{\Delta\varepsilon^p}{2}\right) + C_2 \frac{\Delta\varepsilon^p}{2} + (Q_M - Q_0) \left(1 - \exp\left(-2\beta \frac{\Delta\varepsilon^p}{2}\right)\right) \quad (18)$$

**Table 5**  
Models determination.

Model	monotonic curve	cyclic curve
2AF-1		✓
2AF-2	✓	
AFP-1		✓
AFP-2	✓	
SC	✓	✓

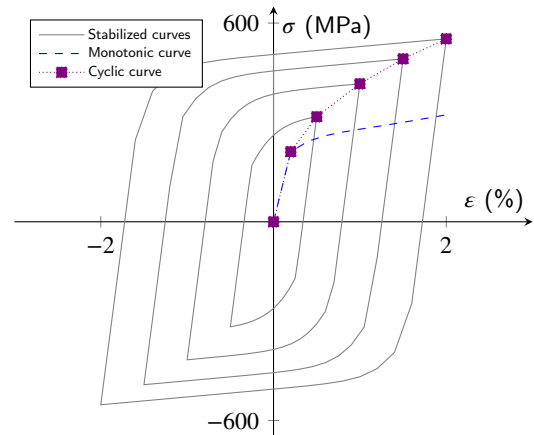


**Figure 7:** Illustration of material curves.

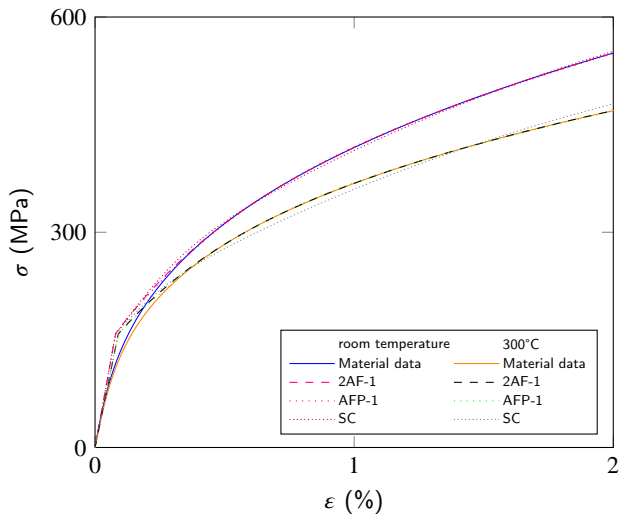


Figure 8: Comparison with cyclic curves.

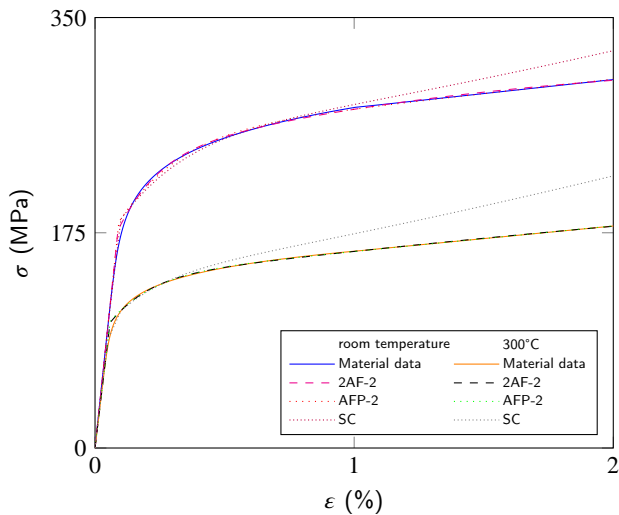


Figure 9: Comparison with monotonic curves.

#### 4. Finite element model

Due to the axisymmetry problem, a 2D finite element model (Fig. 10) is meshed with Visual Mesh software®. Quadratic elements with four Gauss integration points, are used in both electrothermal and thermomechanical simulations. These elements are recommended when plasticity with von Mises criterion (4) is used.

The simulation of thermomechanical effects is divided into two parts. First, the heating by Joule effect is simulated to obtain the temperature distributions over time. The electric potential difference parameter  $\Delta V$  is calibrated in order to obtain the measured temperature over one cycle. Mechanical effects are neglected in the electrothermal simulation.

Once the temperature map calibrated, thermomechanical simulations are performed. Thermal effects are here considered taking temperature-dependent mechanical parameters and using thermal simulation results to calculate the thermal



Figure 10: COThAA mesh.

stresses. Fig. 11 schematizes the interaction between physics phenomena during the simulations.

Constitutive models proposed in section 3.2 and determined in section 3.3 are used to perform thermomechanical simulations. The maximal hoop ratcheting, on the cylinder's external generatrix, is then extracted from the simulations to compare with experimental results. Note that all the simulations described below are performed using the computer code SYSTUS®.

#### 4.1. Electrothermal model

The Joule effect heating appears when the electrical energy produced by high intensity electrical current that flows through a conductive material is converted into thermal energy. This principle that is used to assembly thin metal sheets by welding processes was used to create the thermal stresses of the COThAA experiment. The Joule effect numerical

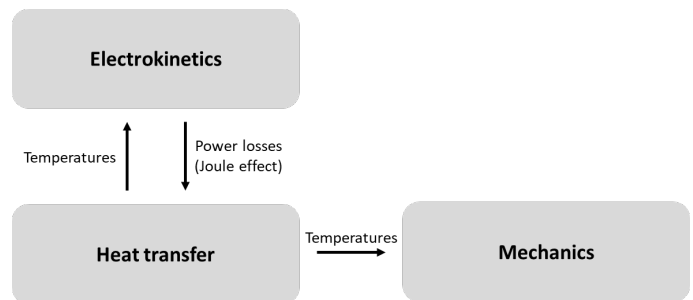


Figure 11: Illustration of COThAA test simulation.



simulation presented hereafter is exhaustively detailed in [36, 37].

Electrothermal proprieties of 316L austenitic stainless steel such as the thermal conductivity, the volumetric mass, and specific heat capacity are temperature-dependent and listed in Table 2.

Concerning the boundary conditions, the natural convection is modelled by means of an exchange coefficient  $h_{air} = 20W/^\circ C.m^2$  and an external environment temperature  $T_{ext} = 20^\circ C$  applied to the cylinder inner and outer walls. The heating by Joule effect is simulated applying an electric potential difference  $\Delta V$  between the bottom and top surface of the COTHAA geometry. The boundary conditions and the electrokinetic loading are showed in Fig. 12.

Unfortunately, we do not have temperature results from test 7, 11 and 12. Thus, their thermal modelling are made by reducing the test 8 heating time to obtain the set temperature observed at the experimental campaign.

## 4.2. Thermomechanical model

As plasticity is considered and model parameters are temperature-dependent, a transient step-by-step calculation is performed. Indeed, the solution of equilibrium equations is time-dependent. The thermomechanical properties, listed in Table 3, and the constitutive models parameters depend on the temperature.

The boundary condition is imposed blocking the axial displacement of the mock-up top surface. The mechanical loading is set by applying a constant internal pressure to the mock-up inner wall and a constant axial stress to the bottom surface. These conditions are illustrated in Fig. 13. The thermal loading is imposed using the temperature cards of the thermal model. Constitutive models, proposed in section 3.2, are used in order to simulate the hoop ratcheting.

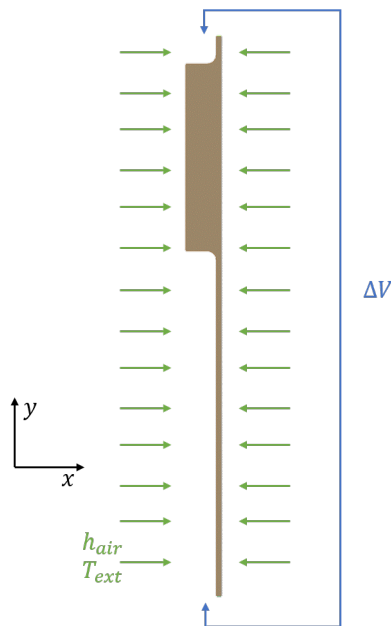


Figure 12: Electrothermal model.

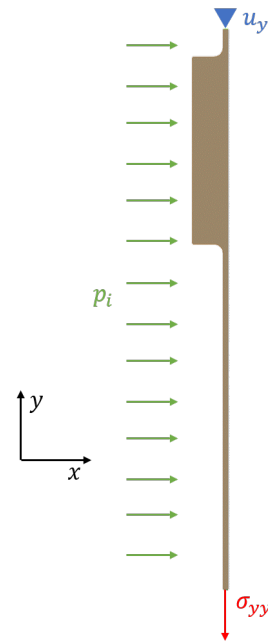


Figure 13: Thermomechanical model.

## 5. Results and discussions

### 5.1. Electrothermal validation

A sensitivity analysis was performed on the electric potential difference parameter  $\Delta V$  in order to reproduce the TC12 experimental information (Fig. 3). In other words, various calculations were carried out to calibrate  $\Delta V$  and to validate the thermal loading. The comparison between calculation and experimental results is presented in the Fig. 14. One can see that the simulation is in good agreement with the experimental results.

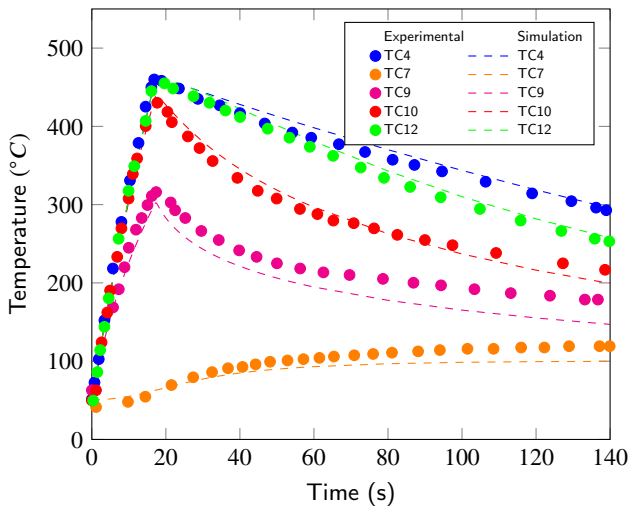
The temperature field of test 8 is showed in Fig. 15. One observes that the simulation reproduces the phenomenon mentioned in section 2.2. Furthermore, as mentioned in section 4.1, the test 8 modelling makes it possible to simulate others COTHAA experiments by changing the heating time. Those time-temperature evolutions are then used to performed thermomechanical calculations.

### 5.2. Evaluation of the constitutive models

In the following section, the experimental hoop ratcheting results and numerical ones are presented and compared.

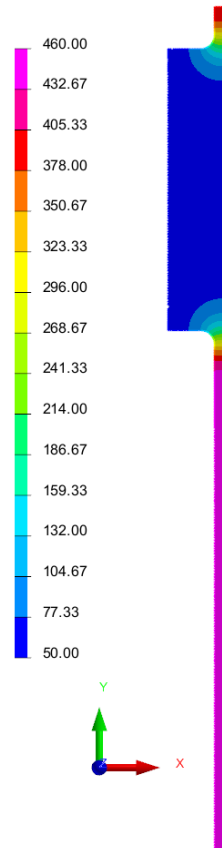
Before proceeding to the results of the simulations, the test 8 configuration at 100th cycle is presented in Fig. 16. Comparing with Fig. 4, one can note that the simulation is able to reproduce the experimental observations.

Fig. 17 shows the ratcheting simulations by 2AF-1 and AFP-1 models along with the test 8 result. The two models underestimate experimental response. Fig. 18 presents the simulations of 2AF-2 and AFP-2 model. During the first ten cycles, it is observed a good correlation between simulation and experimental results, but then the simulations



**Figure 14:** Comparisons of the time-temperature evolution over a cycle.

Test 8 - Temperature (°C)



**Figure 15:** Test 8 temperature field at maximum temperature over one cycle.

overpredict experimental ratcheting. Furthermore, the 2AF-2 model produces a constant ratcheting rate, contrary to the experimental observations.

The simulation with the SC model is showed in Fig. 19. Using the kinetic parameters set to  $b = 15$ ,  $\eta = 0.3$  and  $\beta =$

30, it is observed that the simulation is in good agreement with the ratcheting response of the test 8.

The reason that the kinematic hardening models failed to simulate ratcheting is mainly attributed to model determination. Experimentally speaking, monotonic behaviour is predominant during the first cycles. Then, as the number of cycles increases, the material hardens up and the cyclic behaviour gets predominant. Thus, the plastic modulus is taken very high, for models determined from cyclic curves, or low, for models determined from monotonic curves.

Hence, it is important to consider the cyclic hardening. As SC model considers this phenomenon by using the isotropic hardening rule, the ratcheting simulation is improved. To confirm that SC model is adapted to reproduce ratcheting responses, the simulations of the test 7, 11 and 12 test are performed. The results of all COTHAA test simulations are showed in Fig. 19.

Considering that the thermal loading is deduced from the test 8 and the material properties are taken from a similar material, one can say that SC model is able to reproduce the structural ratcheting of structures under thermomechanical loadings, even though test 7 and 12 are slightly under-predicted. An error of less than 5% is observed between calculations and experimental results (Fig 20).

Test 8 - Radial displacement Ux (mm) - 10x amplified geometry

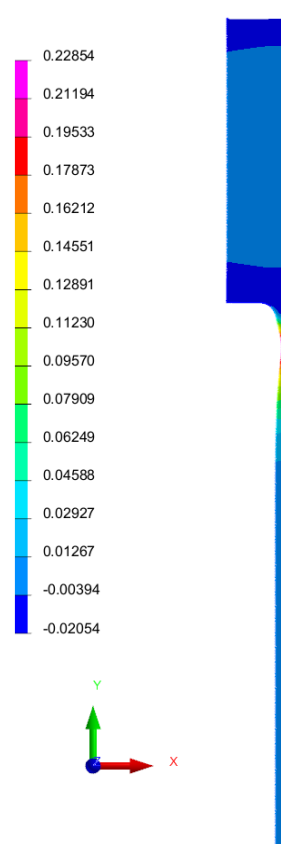


**Figure 16:** Test 8 radial displacement at 100th cycle.

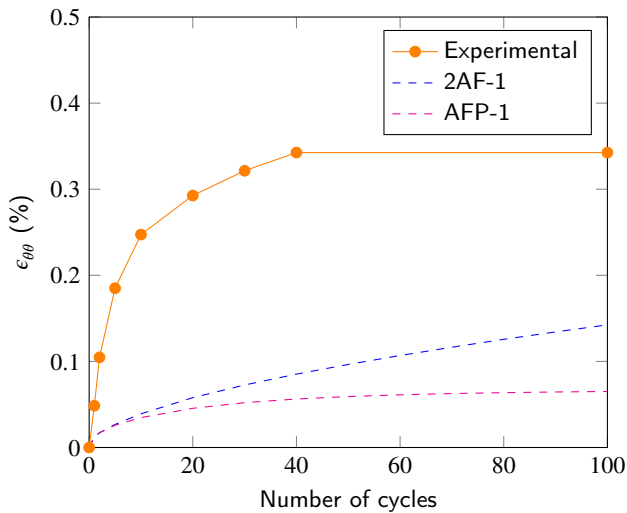


**Figure 17:** Comparisons of the maximal hoop ratcheting over the cycles - 2AF and AFP models determined from isothermal cyclic curves.

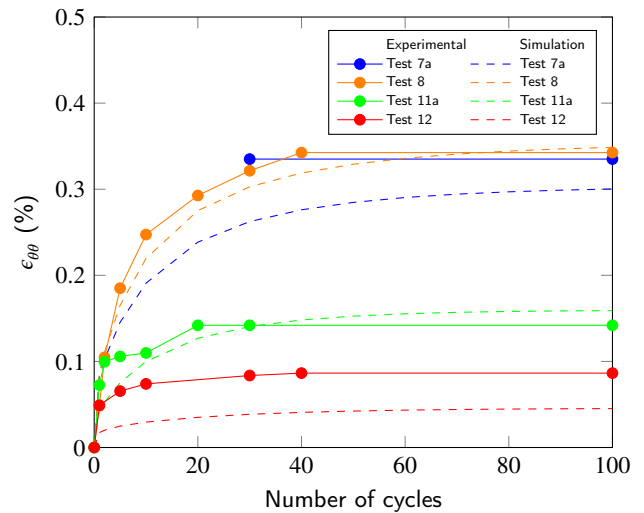


**Figure 19:** Comparisons of the maximal hoop ratcheting over the cycles - SC model determined from both isothermal monotonic and isothermal cyclic curves.

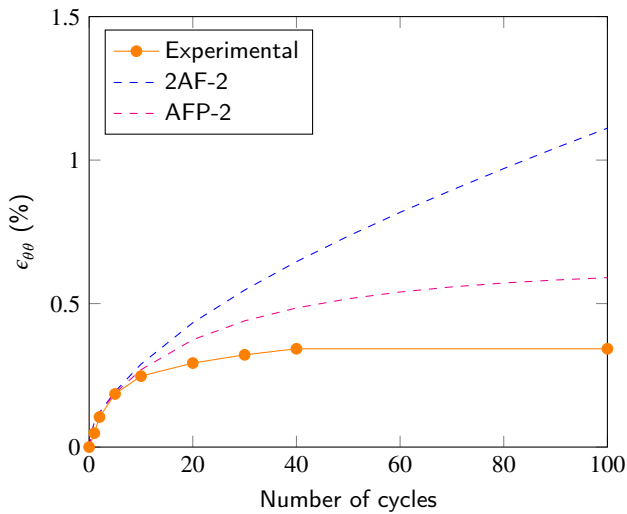


**Figure 18:** Comparisons of the maximal hoop ratcheting over the cycles - 2AF and AFP models determined from isothermal monotonic curves.

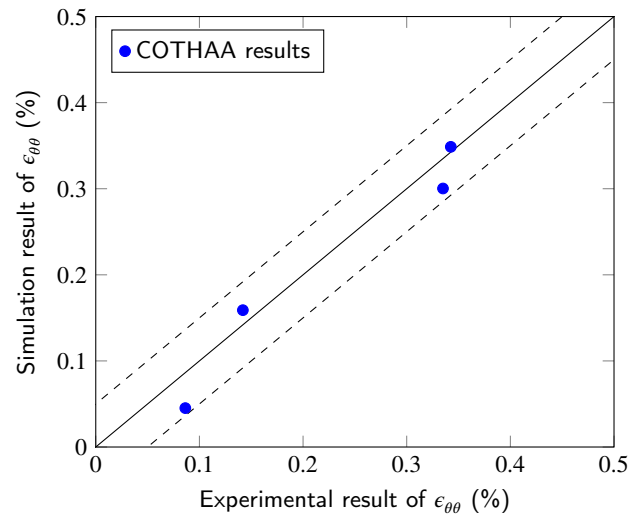


**Figure 20:** Error between simulations and experimental results with SC model.

## 6. Conclusions

This paper is devoted to the structural ratcheting study of a 316L austenitic stainless steel. Numerical analyses of the COTHAA test are performed using the double Armstrong-Frederick model, the Armstrong-Frederick-Prager model and the simplified version of Chaboche model. Furthermore, models determinations are proposed and discussed.

On the one hand, kinematic hardening models underpredict ratcheting when they are determined from cyclic curves. On the other hand, these models overestimate the ratcheting when model's parameters are identified from monotonic tensile curves. These observations indicate that it is necessary to consider the austenitic stainless steel hardening in calculations.

Therefore, the current study proposes a constitutive model that is able to reproduce both the cyclic curves and the monotonic ones. This model is formed of an isotropic hardening rule and two kinematic ones and is determined from both monotonic and cyclic curves. A strategy to determine the model's parameters from material curves is also proposed.

Concerning that model, the results indicate that simulations are found in good agreements as compared to experimental results. Based on these observations, the combination of an isotropic and kinematic hardening is recommended for ratcheting simulation of structures submitted to thermomechanical loadings.

Future work will be focused on a development of a numerical method of speeding up the convergence of non-linear cyclic calculations of structures. The latter will then be

compared with those coming from the direct cycle-by-cycle and the cycle jump technique. Furthermore, an alternative method to assess the thermal structural ratcheting will be proposed and tested on experimental and simulation data.

## References

- [1] A. Benoit, M. H. Maitournam, L. Rémy, and F. Oger. Cyclic behaviour of structures under thermomechanical loadings: Application to exhaust manifolds. *International Journal of Fatigue*, 38:65–74, May 2012.
- [2] Jean Macedo, Stéphane Chapuliot, Jean-Michel Bergheau, Eric Feulvarch, Olivier Ancelet, and Antoine Martin. A Historical Overview of Design Analyses and Experimental Observations of Ratcheting Phenomenon. *ASME 2020 Pressure Vessels & Piping Conference*, October 2020.
- [3] Hartwig Hübel. Basic conditions for material and structural ratcheting. *Nuclear Engineering and Design*, 162(1):55–65, March 1996.
- [4] Jürgen Rudolph, Arturs Kalnins, Andreas Götz, and Roland Hilpert. Local Ratcheting by Elastic-Plastic FEA: Criteria and Code Based Approaches. pages 617–627. American Society of Mechanical Engineers Digital Collection, May 2012.
- [5] Tasnim Hassan and Stelios Kyriakides. Ratcheting of cyclically hardening and softening materials: I. Uniaxial behavior. *International Journal of Plasticity*, 10(2):149–184, January 1994.
- [6] Laurence Portier, Sylvain Calloch, Didier Marquis, and Philippe Geyer. Ratcheting under tension-torsion loadings: experiments and modelling. *International Journal of Plasticity*, 16(3):303–335, January 2000.
- [7] G. Facheris, K. G. F. Janssens, and S. Foletti. Multiaxial fatigue behavior of AISI 316L subjected to strain-controlled and ratcheting paths. *International Journal of Fatigue*, 68:195–208, November 2014.
- [8] Tasnim Hassan and Stelios Kyriakides. Ratcheting of cyclically hardening and softening materials: II. Multiaxial behavior. *International Journal of Plasticity*, 10(2):185–212, January 1994.
- [9] A Gustafsson and M Möller. Experimental and Numerical Investigation of Ratcheting in Pressurized Equipment. *Procedia Engineering*, 130:1233–1245, 2015.
- [10] Navid Moslemi, Mohsen Gol Zardian, Amran Ayob, Norizah Redzuan, and Sehun Rhee. Evaluation of Sensitivity and Calibration of the Chaboche Kinematic Hardening Model Parameters for Numerical Ratcheting Simulation. *Applied Sciences*, 9(12):2578, January 2019. Number: 12 Publisher: Multidisciplinary Digital Publishing Institute.
- [11] Jianbei Zhu, Xu Chen, Fei Xue, and Weiwei Yu. Bending ratcheting tests of Z2CND18.12 stainless steel. *International Journal of Fatigue*, 35(1):16–22, February 2012.
- [12] Syed M. Rahman, Tasnim Hassan, and Edmundo Corona. Evaluation of cyclic plasticity models in ratcheting simulation of straight pipes under cyclic bending and steady internal pressure. *International Journal of Plasticity*, 24(10):1756–1791, October 2008.
- [13] Xiao Chen. Ratcheting Study of Pressurized Straight Z2CND18.12N Austenitic Stainless Steel Pipe under Reversed Bending. *Advanced Materials Research*, 798-799:235–238, September 2013.
- [14] Aritra Sarkar, A. Nagesha, P. Parameswaran, R. Sandhya, and M. D. Mathew. Influence of dynamic strain aging on the deformation behavior during ratcheting of a 316LN stainless steel. *Materials Science and Engineering: A*, 564:359–368, March 2013.
- [15] Yiming Zheng, Bingbing Li, Qite Li, Caiming Liu, and Xu Chen. Ratcheting deformation behavior of 316LN stainless steel under thermomechanical and isothermal loadings. *International Journal of Fatigue*, 138:105718, September 2020.
- [16] Xingyue Sun, Ruisi Xing, Weiwei Yu, and Xu Chen. Uniaxial ratcheting deformation of 316LN stainless steel with dynamic strain aging: Experiments and simulation. *International Journal of Solids and Structures*, 207:196–205, December 2020.
- [17] M. Foroutan, G. R. Ahmadzadeh, and A. Varvani-Farahani. Axial and hoop ratcheting assessment in pressurized steel elbow pipes subjected to bending cycles. *Thin-Walled Structures*, 123:317–323, February 2018.
- [18] Takeo Uga. An experimental study on thermal-stress ratcheting of austenitic stainless steel by a three bars specimen. *Nuclear Engineering and Design*, 26(2):326–335, February 1974.
- [19] Lakhdar Taleb, Michel Cousin, and Jean François Jullien. Metallic structures subjected to cyclic loadings: I. Inadequacy of the elastic analysis for the steady state assessment. *International Journal of Pressure Vessels and Piping*, 75(3):173–180, March 1998.
- [20] C. Couterot, P. Geyer, and J. M. Proix. Experiment and numerical analysis of the NPP pressurizer auxiliary spray line submitted to large thermal shocks; Etude expérimentale et numérique de la ligne d’aspersion auxiliaire du pressuriseur soumise a des transitoires thermiques de forte amplitude. *EDF Report 94-NB-00135*, March 1994.
- [21] M. T. Cabrillat, P. Geyer, P. Robinet, C. Migne, P. Matheron, T. Yuritzinn, and S. Taheri. Benchmark on a thermal ratcheting test. Comparison of different constitutive models. *14th International Conference on Structural Mechanics in Reactor Technology*, 1997.
- [22] M. T. Cabrillat and Y Meziere. Evaluation of ratcheting on experimental tests using simplified design rules. *14th International Conference on Structural Mechanics in Reactor Technology*, 1997.
- [23] William Prager. A New Method of Analyzing Stresses and Strains in Work-Hardening Plastic Solids. *Journal of Applied Mechanics*, 23(4):493–496, December 1956.
- [24] P.J. Armstrong and C.O. Frederick. A Mathematical Representation of the Multiaxial Bauschinger Effect. *CEGB report no RD/BN 731*, 1966.
- [25] J. L. Chaboche. Constitutive equations for cyclic plasticity and cyclic viscoplasticity. *International Journal of Plasticity*, 5(3):247–302, January 1989.
- [26] N. Ohno and J. D. Wang. Kinematic hardening rules with critical state of dynamic recovery, part I: formulation and basic features for ratcheting behavior. *International Journal of Plasticity*, 9(3):375–390, January 1993.
- [27] Z. Mróz. On the description of anisotropic workhardening. *Journal of the Mechanics and Physics of Solids*, 15(3):163–175, May 1967.
- [28] Z. Mróz. An attempt to describe the behavior of metals under cyclic loads using a more general workhardening model. *Acta Mechanica*, 7(2):199–212, June 1969.
- [29] Y. S. Garud. A New Approach to the Evaluation of Fatigue Under Multiaxial Loadings. *Journal of Engineering Materials and Technology*, 103(2):118–125, April 1981.
- [30] RCC-MRx. *Règles de conception et de construction des matériels mécaniques des installations nucléaires hautes températures, expérimentales et de fusion*. AFCEN, 2018 edition, 2018.
- [31] R. H. Bogaard, P. D. Desai, H. H. Li, and C. Y. Ho. Thermophysical properties of stainless steels. *Thermochimica Acta*, 218:373–393, May 1993.
- [32] Shafiqul Bari and Tasnim Hassan. Anatomy of coupled constitutive models for ratcheting simulation. *International Journal of Plasticity*, 16(3):381–409, January 2000.
- [33] J. L. Chaboche, K Dang Van, and G Cordier. Modelization of the strain memory effect on the cyclic hardening of 316L Stainless steel. *SMIRT 5*, 1979.
- [34] J. L. Chaboche and G. Rousselier. On the Plastic and Viscoplastic Constitutive Equations—Part I: Rules Developed With Internal Variable Concept. *Journal of Pressure Vessel Technology*, 105(2):153–158, May 1983.
- [35] J. L. Chaboche. A review of some plasticity and viscoplasticity constitutive theories. *International Journal of Plasticity*, 24(10):1642–1693, October 2008.
- [36] Jean-Michel Bergheau and Roland Fortunier. *Finite Element Simulation of Heat Transfer* | Wiley. Wiley, March 2013.
- [37] Eric Feulvarch and Jean Michel Bergheau. Modeling and Numerical Simulation of Resistance Spot Welding Process. In Richard B.

Hetnarski, editor, *Encyclopedia of Thermal Stresses*, pages 3112–3123. Springer Netherlands, Dordrecht, 2014.